Compact Wideband Folded Dipole Antenna With Multi-Resonant Modes

Wei Hu, *Member, IEEE*, Xuekang Liu, Steven Gao, *Fellow, IEEE*, Lehu Wen, Qi Luo, *Member, IEEE*, Peng Fei, *Member, IEEE*, Yingzeng Yin, *Member, IEEE*, and Ying Liu, *Senior Member, IEEE*

***Abstract*— A compact and wideband folded dipole antenna with multi-resonant modes is presented in this paper. Three resonant modes are obtained by using a modified planar folded dipole and its coupled feeding structure. Incorporating the shorting pins and parasitic patches, multiple resonant modes in the antenna are manipulated, shifted, and then combined to increase the impedance bandwidth. Using this concept, a prototype of a multi-mode folded dipole is designed, fabricated, and measured. The experimental results show that the proposed antenna achieves a bandwidth of 80% from 1.57 to 3.68 GHz, while occupying a compact size of $0.3\lambda_0 \times 0.15\lambda_0 \times 0.05\lambda_0$ (λ_0 is the wavelength in free space at the lowest operating frequency). Furthermore, a simple and effective design to achieve good omnidirectional radiation performance is developed by placing two proposed folded dipoles back to back. The antenna exhibits a flat gain variation of less than 1.27 dB over a broad bandwidth (82%) in the horizontal plane. Such a compact, wideband, planar antenna is a promising candidate for indoor signal coverage, wireless access points, and micro base stations in 2G/3G/4G/5G and WLAN/WiMAX wireless communication systems.**

***Index Terms*— Folded dipole antenna (FDA), multi-resonant modes, omnidirectional radiation, wide bandwidth.**

I. Introduction

With the development of wireless communication technologies, it has become increasingly desirable for modern communication devices to integrate multiple communication standards, such as 2G/3G/4G/5G and WLAN/WiMAX, into one single system. Therefore, antennas with broadband performance are in high demand for multi-standard coverage. Dipole antennas are widely used in wireless communication systems. To achieve broadband operation, various designs of dipole antennas have been reported, such as modifying the shape of the dipole arms [1]–[3], improving feeding methods [4], [5], loading parasitic radiators [6]–[8], and employing magnetoelectric complementary structures [9]–[10]. As a typical transformation of the single dipole, the folded dipole antennas (FDAs) are employed in many applications [11]–[14] owing to the wideband impedance characteristics. Many research works have been carried out [15]–[19] to improve the operation bandwidth of FDA. In [15], by compensating the mutual coupling, a four-element FDA array with 53.2% (1.19–2 GHz) bandwidth is developed at the expense of increasing the size of antenna. By using the formulas in [16], a wideband asymmetric coplanar strip FDA is designed in [17]. Through optimizing the widths of the asymmetric coplanar strip, this FDA exhibits a broad bandwidth of 55%. Besides, by loading different types of slots on 3-D FDAs, 57% and 67% bandwidths are achieved in [18] and [19], respectively. However, these reported antennas suffer unstable gain in their operating bands.

In this paper, a novel multi-resonant mode approach is proposed to enhance the bandwidth of the FDA. This approach is inspired by the dual-resonant cavity model of microstrip antennas [20], [21]. In our design, multiple resonant modes in the antenna are generated, manipulated, shifted, and then combined to increase the operation bandwidth. Through the FDA evolution from a linear model to a planar structure, the 1st-order and 3rd-order modes are manipulated and shifted toward each other. A pair of shorting strips is symmetrically introduced to optimize the input impedances of the two modes. In this way, a wideband planar folded dipole antenna (PFDA) is obtained with dual-resonant modes. To further improve the bandwidth of the dual-mode PFDA, a capacitively coupled feeding structure is employed, which generates a new resonant mode at the higher frequency. Moreover, a pair of parasitic patches is utilized to shift the additional resonance and obtain good impedance matching. Finally, a triple-resonant-mode PFDA is achieved with a broad bandwidth of 80% from 1.57 to 3.68 GHz. To the best knowledge of the authors, it is a new exploration to manipulate, shift, and combine multi-resonant modes to enhance the FDA impedance bandwidth. It is the first time that this approach to design a compact wideband planar antenna based on the multi-mode FDA is presented.

Additionally, omnidirectional radiation performance is also required for many wireless communication applications, such as indoor signal coverage, wireless access points, and micro base stations. Based on the multi-mode PFDA, a simple and effective design to achieve omnidirectional radiation

Manuscript received December 27, 2018; revised May 21, 2019; accepted June 11, 2019. Date of publication July 23, 2019; date of current version October 29, 2019. This work was supported in part by the Young Talent Fund of University Association for Science and Technology in Shaanxi, China, under Grant 20170105, in part by the Natural Science Foundation of Shaanxi, China, under Grant 2018JM6038, in part by EPSRC under Grant EP/N032497/1, Grant EP/P015840/1, and Grant EP/S005625/1, and in part by the Fundamental Research Funds for the Central Universities under Grant RC1902. *(Corresponding authors: Wei Hu; Xuekang Liu.)*

W. Hu, X. Liu, Y. Yin, and Y. Liu are with the National Laboratory of Science and Technology on Antennas and Microwaves, Xidian University, Xi'an 710071, China (e-mail: weihu.xidian@ieee.org; hcmx1994@gmail.com).

S. Gao, L. Wen, and Q. Luo are with the School of Engineering and Digital Arts, University of Kent, Canterbury CT2 7NT, U.K. (e-mail: s.gao@kent.ac.uk).

P. Fei is with the Institute of Radio Metrology and Measurement, Beijing 100854, China (e-mail: feipeng@ieee.org).

Color versions of one or more of the figures in this article are available online at http://ieeexplore.ieee.org.

Digital Object Identifier 10.1109/TAP.2019.2925188

performance is developed by placing two of the proposed PFDAs back to back. The resulting antenna exhibits good omnidirectional radiation patterns in the horizontal plane with flat gain variation of less than 1.27 dB. The presented compact broadband antenna is a good candidate for indoor signal coverage, wireless access points, and micro base stations in 2G/3G/4G/5G (1.7–2.7 GHz, 3.4–3.6 GHz), WLAN 2.4 GHz, and WiMAX 2.5/3.5 GHz applications.

II. Antenna Configuration and Working Principle

A. Antenna Configuration

The configuration of the proposed multi-mode FDA is shown in Fig. 1. The antenna has a four-layer configuration and it is printed on three F4B substrates (relative dielectric permittivity $\varepsilon_r = 2.2$, loss tangent $\tan\delta = 0.001$). These substrates have the same size of 60×30 mm^2, and the thicknesses of them are 0.5, 1.5, and 0.5 mm from top to bottom. There are two air layers between the substrates. The planar folded dipole is composed of two separate rectangular coppers on Sub 2, a rectangular copper sheet on Sub 3, and four rows of shorting pins that connect these two layers. Besides, a pair of parasitic patches is symmetrically etched on Sub 1. To excite the antenna, a planar capacitively coupled feeding strip (CFS) is used. For practical implementation, a 50 Ω SMA connector is mounted below the antenna. The inner conductor is connected to the feeding strip through Sub 3, and its outer conductor is soldered to the metal sheet on the bottom side of Sub 3. To obtain the impedance and radiation performances, the antenna is simulated by using the ANSYS High Frequency Structure Simulator (HFSS).

B. Shift of the Resonant Modes of a Folded Dipole

A linear folded dipole can be analyzed by assuming that its current is decomposed into a transmission line mode and an antenna mode [22], [23]. The input impedance of the FDA is calculated by

$$Z_{in} = \frac{4Z_t Z_d}{2Z_d + Z_t} \tag{1}$$

where Z_t is the input impedance of transmission line mode, and Z_d is the input impedance of a regular dipole. Z_t and Z_d are obtained from

$$Z_t = j\frac{\eta}{\pi}\ln\left[\frac{g+\sqrt{g^2-d^2}}{d}\right]\tan\left(\frac{kl}{2}\right) \tag{2}$$

$$Z_d = \frac{R_r + jX_m}{\sin^2\left(\frac{kl}{2}\right)} \tag{3}$$

where g is the spacing between the two larger sides, d is the diameter of the FDA, l is the length of FDA's larger sides, and R_r and X_m are the input resistance and reactance of the linear dipole, respectively [23].

In this design, the length l of a linear FDA is chosen to be 60 mm, which is the half wavelength of 2.2 GHz. Substituting $l = 60$ mm, $g = 6$ mm, and $d = 0.5$ mm into (1)–(3), the frequency response of the FDA's input impedance is calculated and shown in Fig. 2. The widely used operating band of the FDA is at the range where its input impedance is approximately 300 Ω [23], as indicated by the shaded area around 2.2 GHz in Fig. 2. Note that there are two additional

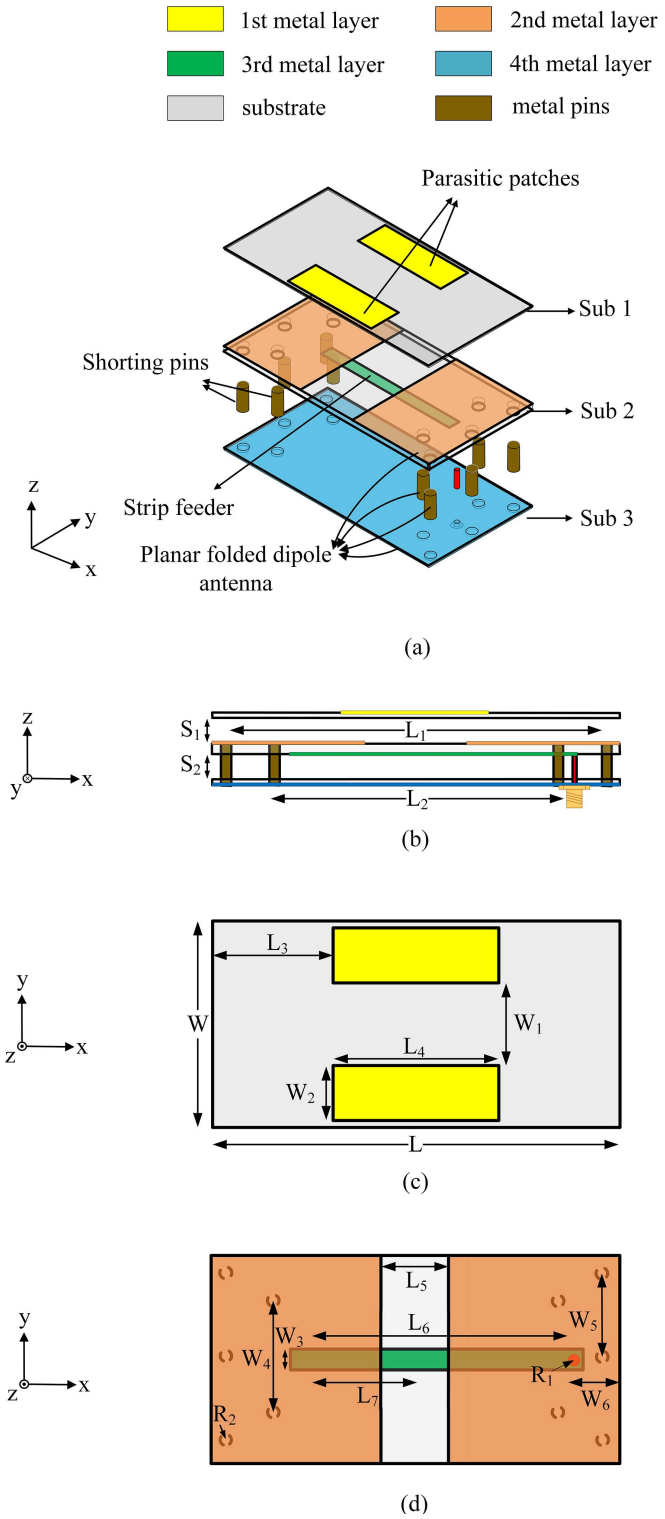

Fig. 1. Configuration of the proposed antenna. (a) 3-D view, (b) side view, (c) top view of Sub 1, and (d) top view of Sub 2. Dimensions are L = 60, $L_1 = 54$, $L_2 = 42$, $L_3 = 19$, $L_4 = 22$, $L_5 = 15$, $L_6 = 37$, $L_7 = 15$, W = 30, $W_1 = 12$, $W_2 = 8$, $W_3 = 2.8$, $W_4 = 14$, $W_5 = 12$, $W_6 = 7$, $R_1 = 0.5$, $R_2 = 1.4$, $S_1 = 4$, and $S_2 = 4$ (unit: millimeters).

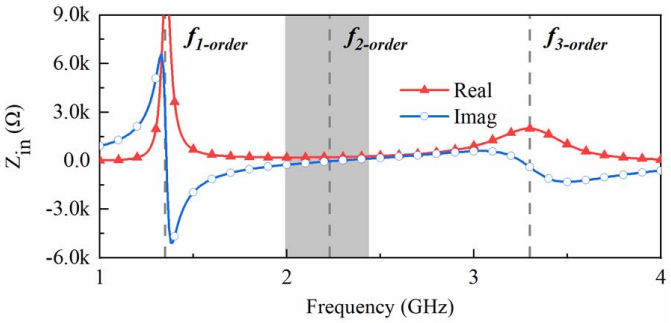

Fig. 2. Calculated input impedance of the linear FDA.

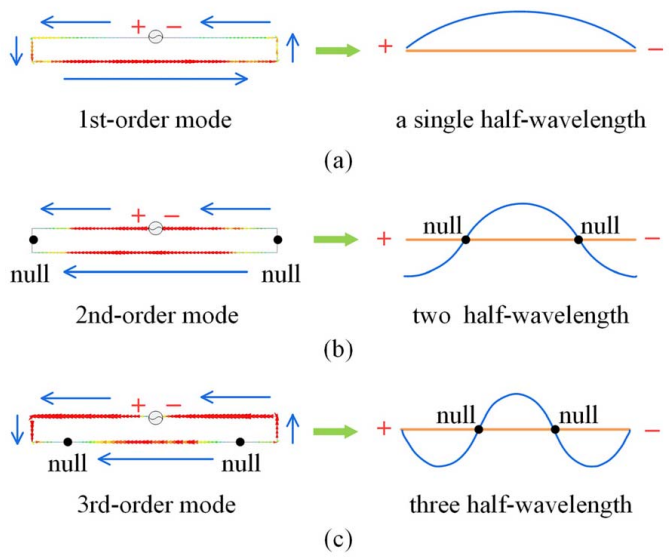

Fig. 3. Schematic of the 1st-order, 2nd-order, and 3rd-order modes of the linear FDA at (a) 1.3, (b) 2.2, and (c) 3.3 GHz.

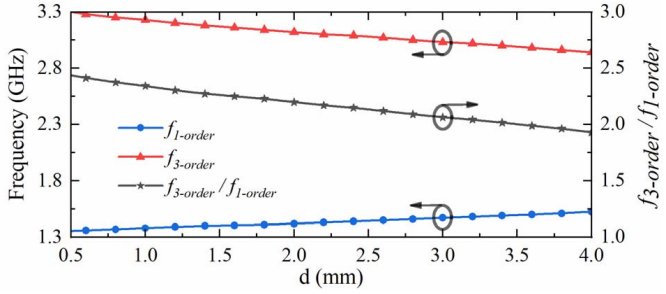

Fig. 4. Calculated $f_{1-order}$, $f_{3-order}$, and $f_{3-order}/f_{1-order}$ as the functions of d.

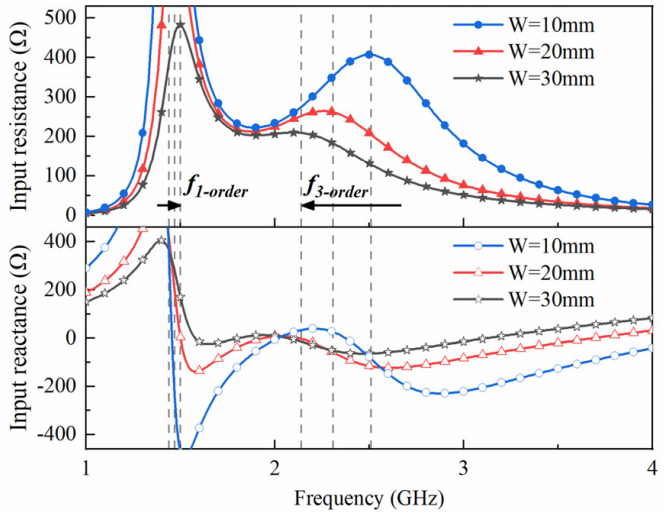

Fig. 5. Simulated input impedances of the PFDA for various W.

resonances appeared on both sides of the original working band. In order to illustrate the operation principle of the linear FDA, Fig. 3 presents the schematic diagram of three different current modes. From the vector current distributions in Fig. 3(a)–(c), it can be seen that three current modes resonated at 1.3, 2.2, and 3.3 GHz represent the 1st-order, 2nd-order, and 3rd-order modes, which indicate half, one, and one and a half wavelength modes along the antenna, respectively. However, these modes are far away from each other, and the input impedances around $f_{1-order}$ and $f_{3-order}$ are very high.

The 1st-order and 3rd-order modes of FDA can be manipulated and shifted by varying the diameter d of the folded dipole. By calculating the first resonant frequency and the third resonant frequency based on (1)–(3), the relationship between $f_{1-order}$, $f_{3-order}$, and d can be expressed in an intuitive way as follows:

$$f_{1-order} = F_1(d) \tag{4}$$

$$f_{3-order} = F_3(d). \tag{5}$$

The calculated $f_{1-order}$, $f_{3-order}$, and $f_{3-order}/f_{1-order}$ as the functions of d are shown in Fig. 4. It shows that $f_{1-order}$ is a monotonically increasing function of d and $f_{3-order}$ is a monotonically decreasing function of d, within the range of 0.5–4.0 mm. This also reveals that the ratio of $f_{3-order}$ to $f_{1-order}$ is reduced as d increases, which predicts that the two resonant modes will be shifted toward each other by increasing the diameter of the FDA. However, due to the structural constraint of the linear FDA, the diameter d cannot be larger than the spacing g between the two larger sides to further decrease $f_{3-order}/f_{1-order}$.

To make the 1st-order and 3rd-order modes closer together, the structure of the FDA is evolved from the linear model to a planar structure. Increasing the width of the PFDA can have the same effect as the increase of the FDA diameter [23]. In this way, the 1st-order and 3rd-order modes can be manipulated and shifted toward each other in a greater extent, which leads to a wideband response of the multi-mode FDA. Fig. 5 shows the simulated input impedance of the PFDA. When increasing the width W, it can be seen that the first resonance of the input impedance moves to the higher frequency, while the third resonance shifts to the lower frequency. The 1st-order and 3rd-order modes of the PFDA are shifted toward each other, and the ratio of the two modes can be manipulated by adjusting the width W. Besides, the increase in the PFDA width contributes to the reduction in the input resistance. Fig. 6 shows the simulated input resistances and resonant frequencies of the 1st-order and 3rd-order modes vary

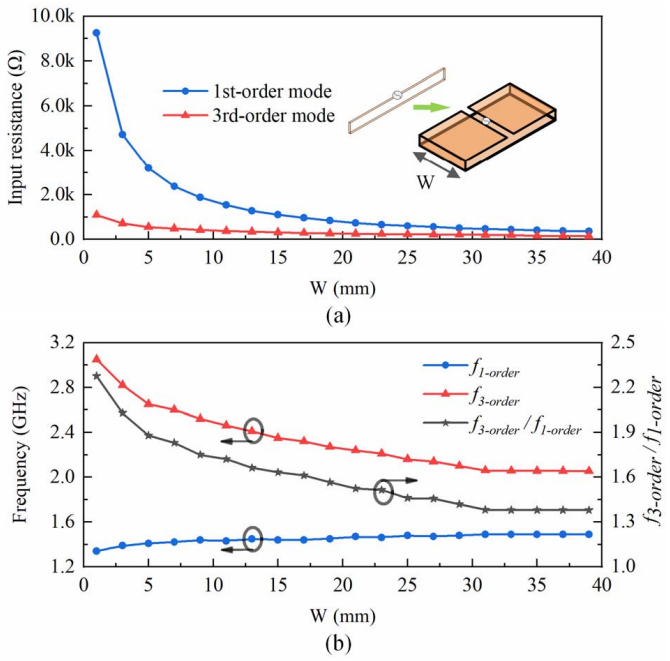

Fig. 6. (a) Simulated input resistances and (b) resonant frequencies and $f_{3-order}/f_{1-order}$ as a function of W at the 1st-order and 3rd-order modes.

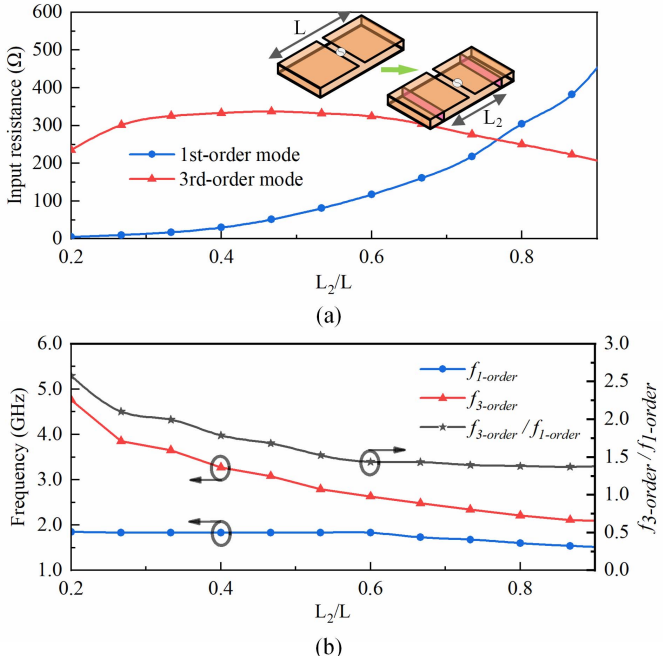

Fig. 7. (a) Simulated input resistances and (b) resonant frequencies and $f_{3-order}/f_{1-order}$ as a function of L_2/L at the 1st-order and 3rd-order modes.

with the different W. By increasing the width W to 40 mm, the input resistances for both resonant modes significantly decrease. Meanwhile, the ratio of $f_{3-order}$ to $f_{1-order}$ is also notably reduced as W increases. The $f_{3-order}/f_{1-order}$ steadily approaches the minimum value of 1.4 after W reaches 30 mm. Considering the miniaturization of the antenna, the width of PFDA is chosen to be 30 mm in the design.

In conclusion, through the FDA evolution from the linear model to the planar structure, the 1st-order and 3rd-order modes can be manipulated and shifted toward each other, and the input resistances of the two modes are also reduced at the same time. However, owing to an initial difference in the input resistance of the linear FDA at the 1st-order and 3rd-order modes in Fig. 2, the resistance difference between the two modes is still large, about 300 Ω.

C. Optimizing the Multi-Mode Input Impedance

In order to optimize the input impedance of the 1st-order and 3rd-order modes, a pair of shorting strips is symmetrically introduced in the design. As shown in Fig. 7, it can be seen that the input resistances at the 1st-order and 3rd-order modes can be manipulated by controlling the distance L_2 between the shorting strips, especially for the 1st-order mode. To adjust the input impedances of the two modes, the value of $L_2/L = 0.75$ is selected with the same input resistance for the 1st-order and 3rd-order modes of PFDA and a minimum ratio of $f_{3-order}/f_{1-order}$ is maintained. By comparing the resistances of PFDA with and without the shorting strips in Fig. 8, it can be observed that the input resistances difference between the two modes becomes small after introducing a pair of shorting strips with $L_2/L = 0.75$, and the maximum values of dual-mode input resistances are close to 260 Ω.

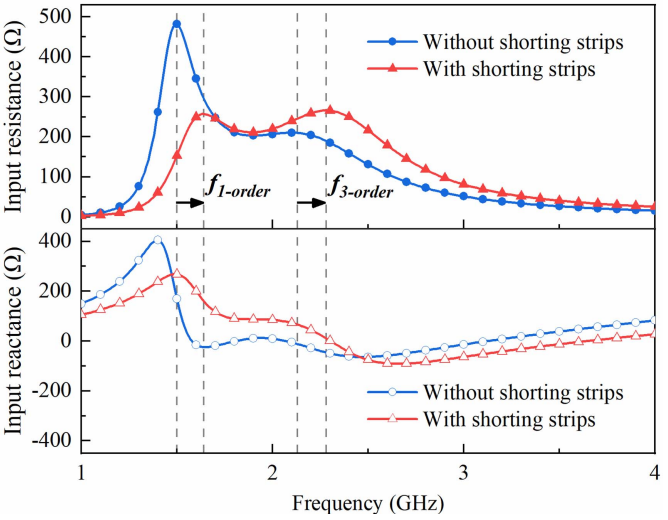

Fig. 8. Simulated input impedances of the PFDA without and with shorting strips when $L_2/L = 0.75$.

Thus, a conclusion can be drawn that the shorting strips play a critical role in adjusting and optimizing the impedance properties of the two resonant modes. As mentioned above, by employing the planar configuration with two shoring strips, the 1st-order and 3rd-order modes of the PFDA are manipulated, shifted, and then combined.

To further investigate the operation mechanism of the PFDA, the surface current distributions of PFDA are given in Fig. 9. At the 1st-order mode, the large current density is observed along the bottom side of the PFDA, with and without the introduced shorting strips. The surface current distributions exhibit a single half-wavelength resonance, which refers to the 1st-order mode of the antenna, whereas three half-wavelength distributions are observed along the whole PFDA for the

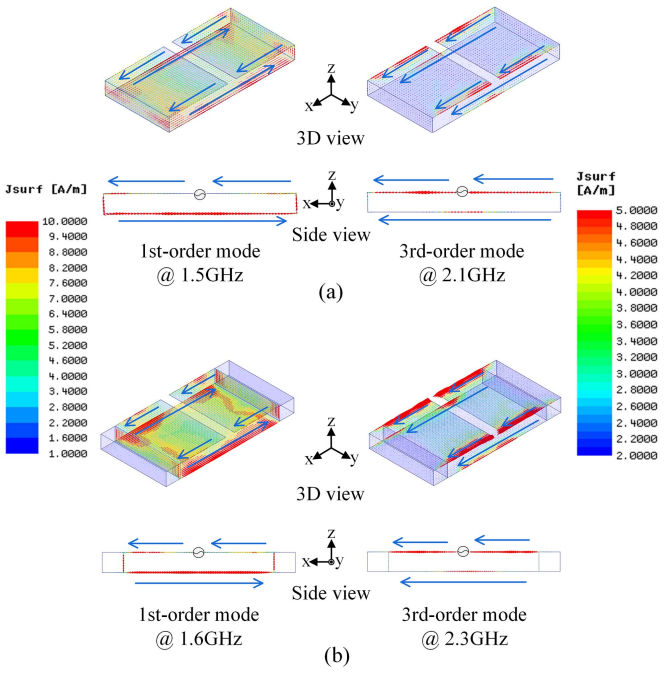

Fig. 9. Surface current distributions of the PFDA (a) without and (b) with shorting strips.

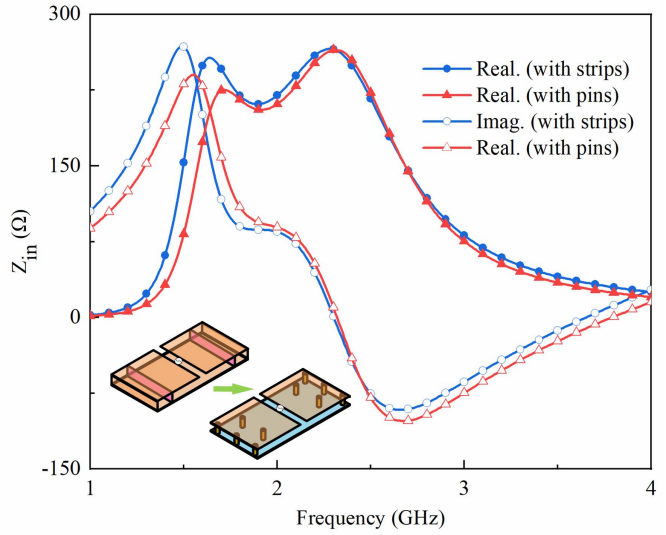

Fig. 10. Simulated input impedances of the PFDA with shorting strips and with shorting pins.

3rd-order mode excitation. It can be seen that the surface current distributions are mainly concentrated along the edges of the PFDA. The observed current distributions are consistent with the design concept, which validate the dual-resonant modes of the antenna. Besides, owing to the introduction of shorting strips, the resonant current paths of PFDA along the x-axis are shortened at both the 1st-order and 3rd-order modes. This leads to the two modes shifting toward the higher frequency simultaneously as shown in Fig. 8. It is worth noting that the ratio between $f_{3-order}$ and $f_{1-order}$ remains almost unchanged because the shift of the two resonant modes is synchronous toward the higher frequency.

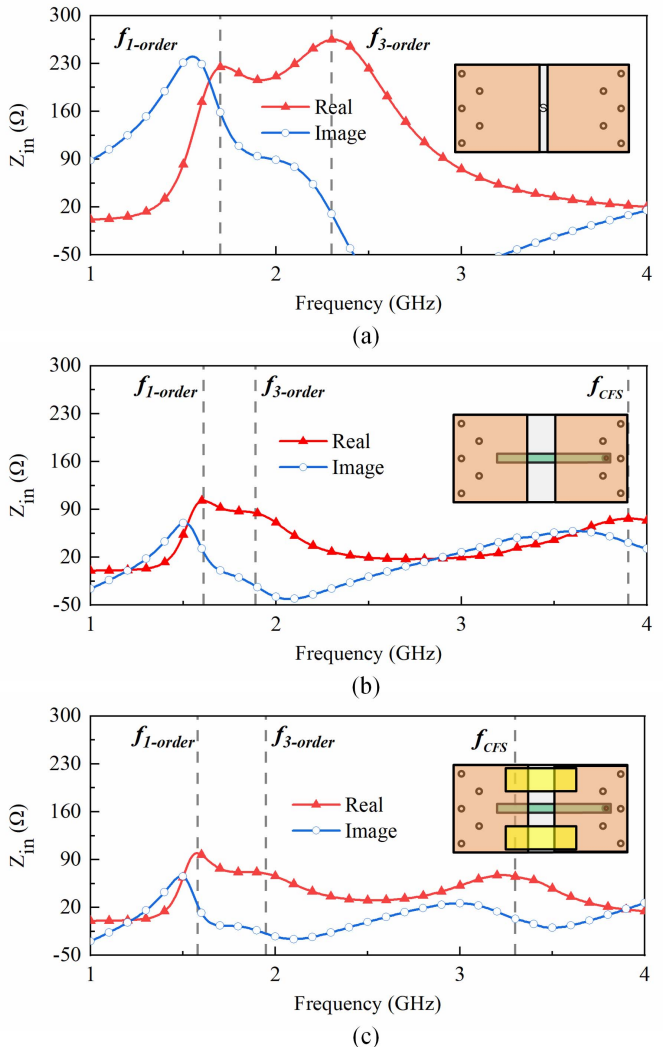

Fig. 11. Simulated input impedances of various PFDAs involved in the design evolution process. (a) Ideally fed antenna. (b) Coupled fed antenna. (c) Coupled fed antenna with parasitic patches.

D. Feeding and Matching Methods

To facilitate the antenna fabrication with PCB technology, four rows of shorting pins are applied in the design to replace the shorting strips and metal side frames. As shown in Fig. 10, it is clear that the use of the shorting pins has little effect on the input impedance of the dual-mode PFDA.

In order to further enhance the bandwidth of the dual-mode PFDA and improve its impedance matching to 50 Ω, effective feeding and matching methods for PFDA are developed.

Fig. 11(a) shows the simulated input impedance of the dual-mode PFDA, which is driven by an ideal lumped port in the simulation by using the ANSYS HFSS. The lumped port connects the two open ends of PFDA with a gap of 4 mm. Note that the input impedance of the dual-mode ideal-fed PFDA exhibits strong inductive component around the 1st-order mode in Fig. 11(a). To obtain good impedance matching, a Γ-shaped coupled feeding structure is employed in Fig. 11(b), which consists of a rectangular feeding strip and an inner conductor of 50 Ω SMA connector. By using this feeding structure, the energy can be coupled to two open ends of PFDA

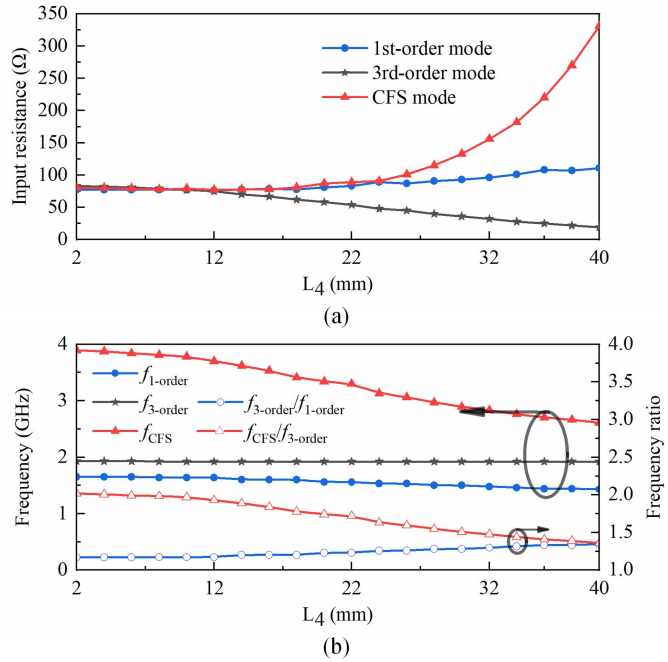

Fig. 12. (a) Simulated input resistances and (b) resonant frequencies and corresponding ratios as a function of L_4 at the 1st-order, 3rd-order, and CFS modes.

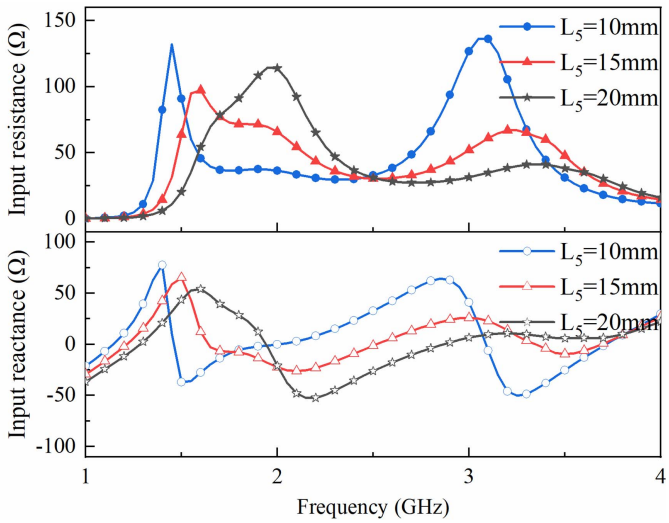

Fig. 13. Simulated input impedances of the proposed antenna for various L_5.

through the feeding strip to excite the antenna. In this way, a capacitive compensation can be provided by the overlapping areas between the feeding strip and the top side of the PFDA. Through the use of this capacitively coupled feeding structure, the input reactance can be decreased from 160 to 30 Ω, while the input resistance is reduced from 240 to 100 Ω, as shown in Fig. 11(b). Moreover, a new resonance at 3.8 GHz is introduced by the CFS. However, the additional CFS resonant mode is too far away from the 1st-order and 3rd-order modes.

To shift the CFS mode toward the two original modes, a pair of parasitic patches is introduced in Fig. 11(c). The effects of the patch length L_4 on the input impedances and the resonant frequencies of the three modes are illustrated in Fig. 12. It is

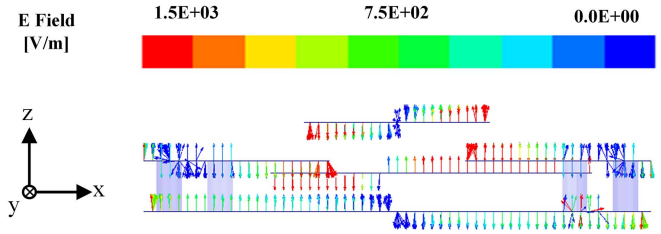

Fig. 14. Electric field distributions of the proposed PFDA at 2.2 GHz.

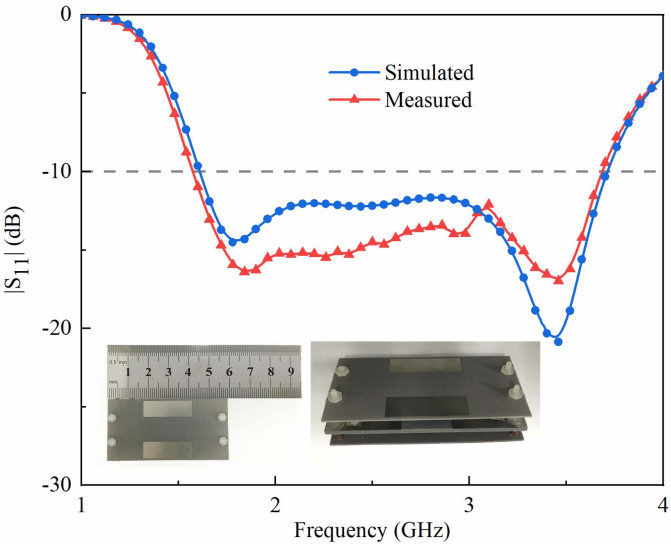

Fig. 15. Measured and simulated reflection coefficients for the proposed antenna.

worth noting that after L_4 increases to 22 mm, the input resistances of 3rd-order mode and CFS mode dramatically change in different ways. The resistance in the CFS mode sharply increases to more than 300 Ω, while the resistance of the 3rd-order mode slowly falls below 50 Ω. Considering the impedance matching and the uniform frequency ratios between the resonant modes, the length L_4 of parasitic patches is chosen to be 22 mm as the optimized value.

Besides, in this design, the gap width L_5 between the two open ends of PFDA can greatly affect the input impedance characteristics, as shown in Fig. 13. It can be observed that as L_5 increases, the resonant modes of the FPDA shift to the higher frequencies. When $L_5 = 15$ mm, the smallest resistance variation range can be obtained across the whole operating frequency band. Therefore, to realize the wideband impedance matching, the value of $L_5 = 15$ mm is selected in this design. The simulated results indicate that the resonant frequencies and the resistance variation range can be simultaneously controlled by adjusting the gap width L_5.

Fig. 14 shows the electric field distribution to provide another insight into the operating principle of the feeding structure. It can be observed that, through the feeding strip, the electric field is coupled to the two open ends of the folded dipole. The electric fields on the left and right sides of the antenna are excited with the same amplitude but opposite phase. The equivalent capacitive loading is formed by coupling the electric fields on the parallel overlapping areas between

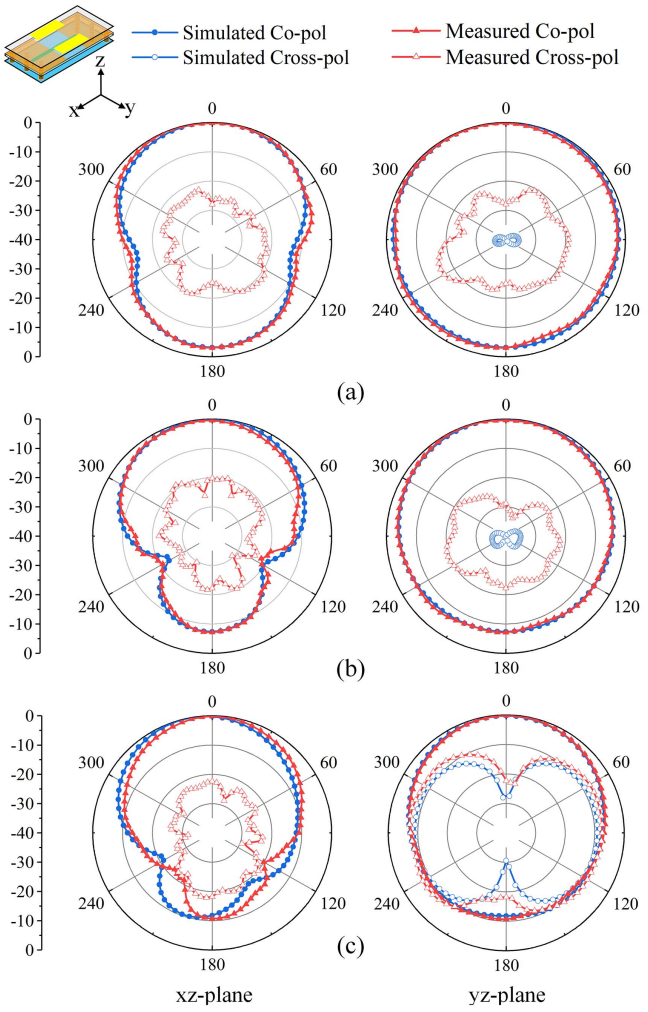

Fig. 16. Measured and simulated normalized radiation patterns for the proposed antenna at (a) 1.6, (b) 2.6, and (c) 3.6 GHz.

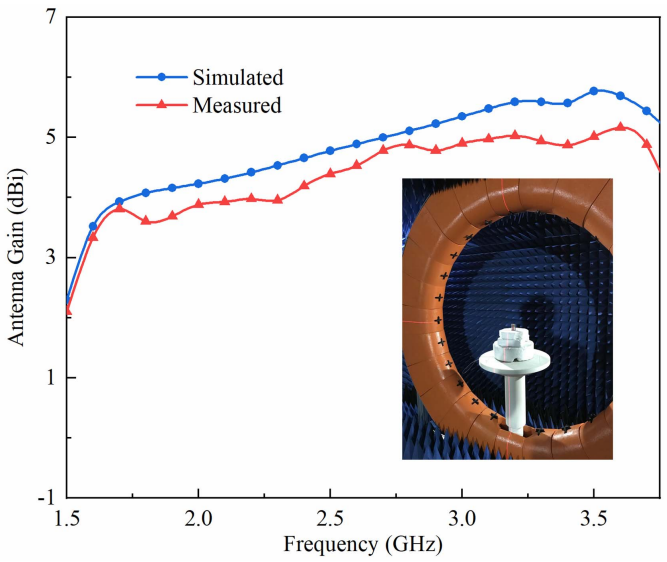

Fig. 17. Measured and simulated peak gains for the proposed antenna.

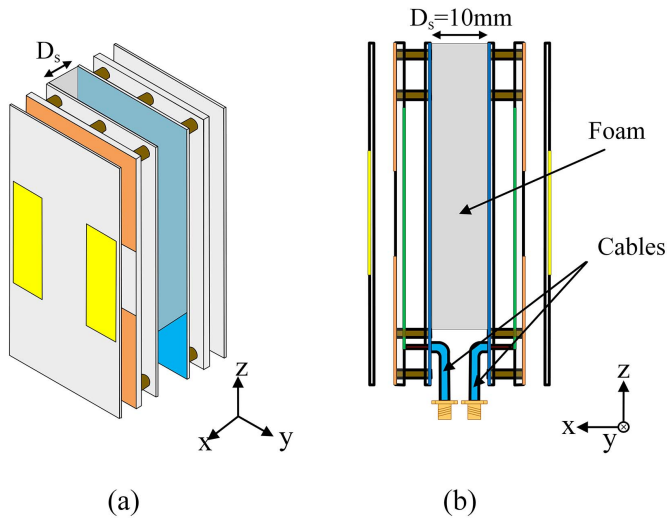

Fig. 18. Configuration of the back-to-back PFDAs. (a) 3-D view. (b) Side view.

the feeding strip and the top side of the PFDA. As mentioned above, by employing the capacitively CFS and parasitic patches, the proposed antenna can realize good triple-mode operation with wideband impedance characteristics.

III. Results and Discussion

A. Multi-Mode PFDA

To validate the above design concept, a multi-mode folded dipole was designed, fabricated, and measured. The simulated and measured reflection coefficients are plotted in Fig. 15. Reasonable agreement between the experimental and the simulated results is obtained. The multiple resonant modes are excited to achieve a good impedance matching for the bandwidth of 80% from 1.57 to 3.68 GHz for $|S_{11}| < -10$ dB, which covers the operating bands for the 2G/3G/4G/5G and WLAN/WiMAX applications.

The radiation characteristics including radiation patterns and antenna gains were measured in a near-field antenna measurement system at Xidian University. Fig. 16 shows the measured and simulated far-field normalized radiation patterns in the *xz* plane and *yz* plane at 1.6, 2.6, and 3.6 GHz. Because of the inherent asymmetry in the *yz* plane, the PFDA exhibits a quasi-omnidirectional pattern with maximum gain in its boresight direction (*z*-axis). As the frequency increases from 1.6 to 3.6 GHz, the front-to-back ratio of the radiation pattern increases from 3 to 10 dB. Besides, it is observed that the proposed antenna has bidirectional radiation in the *xz* plane. The simulated and measured antenna gains are presented in Fig. 17. A stable gain around 4.1 dBi is achieved over the operating band.

Table I compares the proposed antenna with the FDAs reported in recently published papers. A compact vertically stacked FDA with 12% bandwidth is proposed in [13] by utilizing a multi-layer PCB technology. In [14], a planar antenna comprising two folded dipoles obtains a very stable gain around 4 dBi with 20% bandwidth. By compensating the mutual coupling effects, a four-element FDA array achieves a 53% bandwidth at the expense of the increased overall size [15]. By using the formulas in [16], an asymmetric

TABLE I
COMPARISON OF THE FDAS

Ref.	Dimensions (λ_0)	Impedance Bandwidth	Peak gain (dBi)
[13]	0.44×0.44×0.07	12% 26.30-29.75 GHz	5.51
[14]	1.17×0.31×0.01	20% 5.07-6.16 GHz	4.2-4.6
[15]	0.31×0.34×0.11	53% 1.19-2.00 GHz	0.3-1.2
[17]	0.36×0.16×0.00	55% 1.23-2.17 GHz	2.2-2.5
[18]	0.24×0.10×0.05	57% 1.03-1.85 GHz	2.0-5.0
[19]	0.24×0.08×0.04	67% 1.10-2.20 GHz	1.0-4.6
This work	**0.30×0.15×0.05**	**80% 1.57-3.68 GHz**	**3.3-4.9**

* λ_0 is the wavelength at the lowest operating frequency in free space.

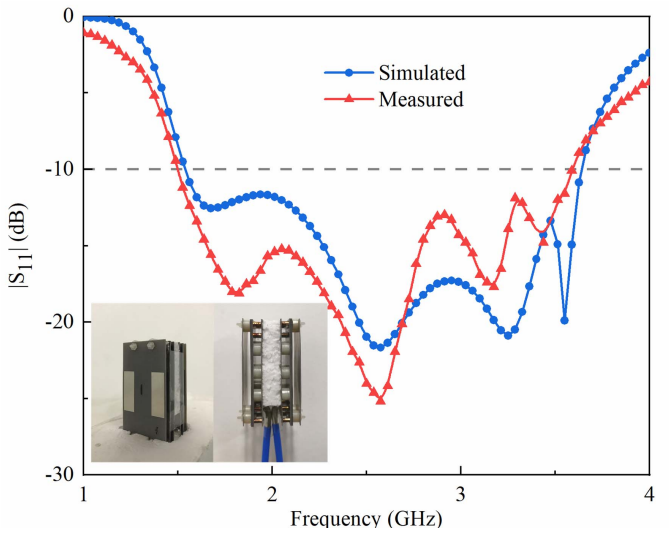

Fig. 19. Measured and simulated reflection coefficients for the back-to-back PFDAs.

coplanar strip FDA is designed with a self-balanced impedance property, exhibiting 55% bandwidth [17]. In [18] and [19], by loading different types of slots on 3-D FDA, 57% and 67% bandwidths are achieved in compact sizes, respectively. However, these antennas suffer unstable gain in their operating bands. Compared to these antennas, the proposed multi-mode PFDA exhibits the widest bandwidth of all the FDAs while achieving a compact size.

B. Back-to-Back PFDAs

Based on the multi-mode PFDA, a design to achieve omni-directional radiation performance is developed in this section.

As shown in Fig. 18, two identical PFDAs are placed back to back along the *z*-axis. The back-to-back PFDAs are fed by two 50 Ω semirigid coaxial cables. The inner conductor of the coaxial cable is connected to the feeding strip, while the outer

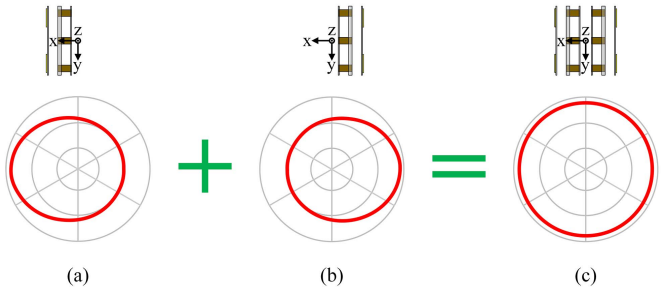

Fig. 20. Operating principle of back-to-back PFDAs with omnidirectional radiation pattern at the *xy* plane. PFDA radiates toward (a) $+x$-axis direction and (b) $-x$-axis direction. (c) Back-to-back PFDAs with omnidirectional radiation.

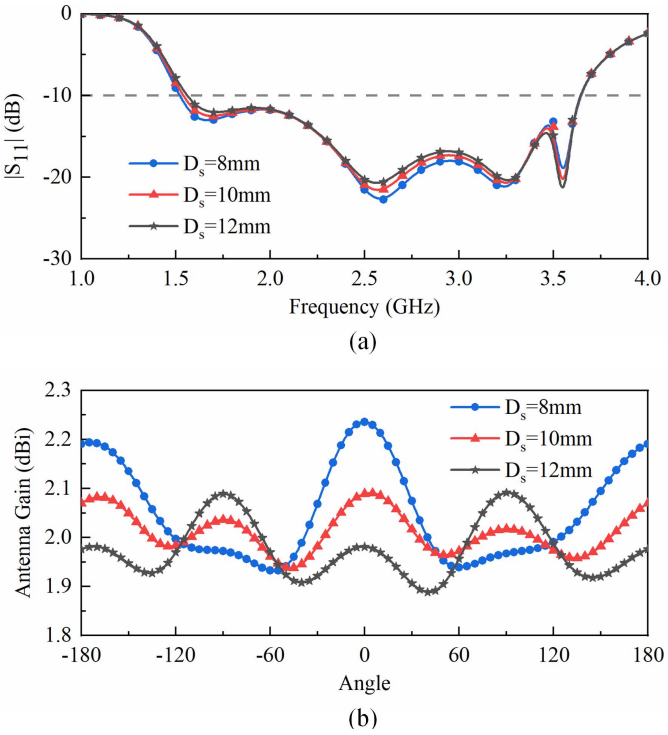

Fig. 21. (a) Simulated reflection coefficients and (b) simulated gain variations in the horizontal plane for various D_s.

conductor is soldered to the metal sheet on the back. A thin layer of foam ($\varepsilon_r = 1.1$) with a thickness D_s of 10 mm is employed to maintain a separation distance between the two PFDAs. The simulated and measured reflection coefficients of the antenna are shown in Fig. 19. Multi-resonant modes are excited to realize a broad bandwidth of 82% (1.5–3.59 GHz). An additional resonance appeared at 3.5 GHz is mainly caused by the mutual couplings between the two PFDAs.

Additionally, the operating principle of the back-to-back PFDAs with omnidirectional radiation pattern is given in Fig. 20. It is known that the PFDA itself has a quasi-omnidirectional radiation pattern with maximum gain in the boresight direction (x-axis) as shown in Fig. 20(a). Also, the antenna gain gradually decreases from $+x$-axis to $-x$-axis. When adding the other PFDA shown in Fig. 20(b) back to back, the gain near the y-axis is enhanced, while the gain in the x-axis direction is almost unchanged. This leads to a more uniform pattern in the xy plane, resulting

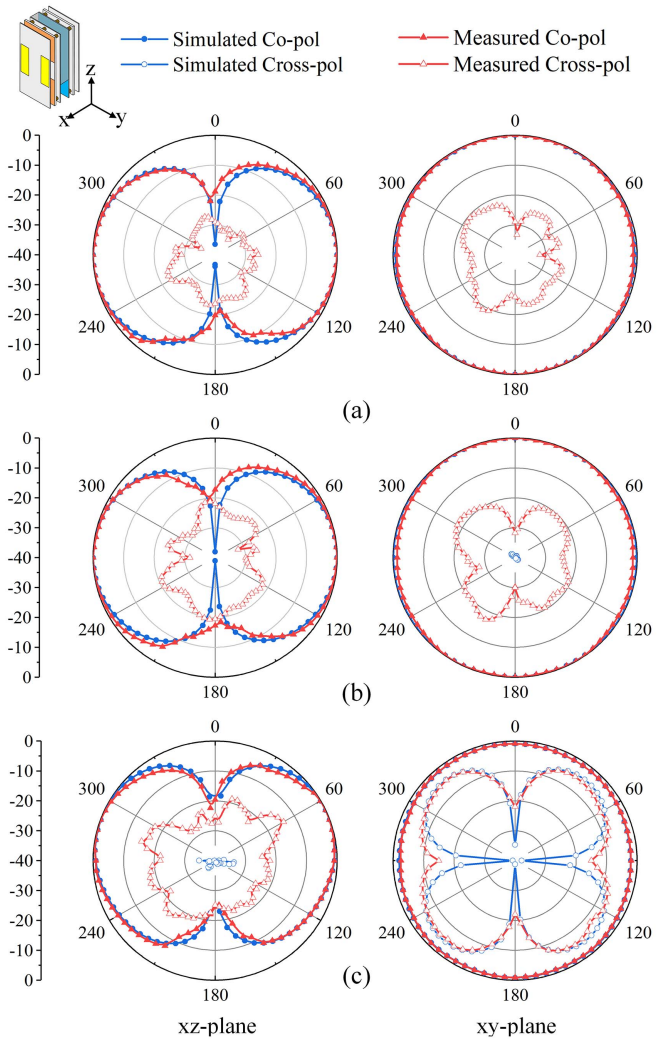

Fig. 22. Measured and simulated normalized radiation patterns for the back-to-back PFDAs at (a) 1.6, (b) 2.6, and (c) 3.6 GHz.

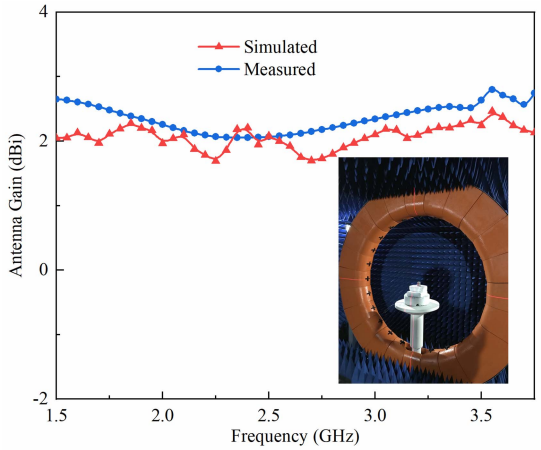

Fig. 23. Measured and simulated peak gains for the back-to-back PFDAs.

TABLE II
COMPARISON OF THE OMNIDIRECTIONAL ANTENNAS

Ref.	Dimensions (λ_0)	Impedance Bandwidth	Gain Variations (dB)
[14]	0.31×1.17×0.01	20% 5.07-6.16 GHz	<2
[17]	0.36×0.16	55% 1.23-2.17 GHz	<4
[24]	3.56×0.53×0.04	11% 13.36-14.98 GHz	<0.7
[25]	0.39×0.39×0.17	53% 1.95-3.35 GHz	<0.7
[26]	0.38×0.38×0.27	152% 0.82-6.00 GHz	<5
[27]	0.24×0.24×0.24	194% 0.45-28.40 GHz	<5
Back-to-back PFDAs	**0.30×0.15×0.13**	**82% 1.50-3.59 GHz**	**<1.27**

*λ_0 is the wavelength at the lowest operating frequency in free space.

in an omnidirectional pattern as shown in Fig. 20(c). Fig. 21 illustrates the effect of the distance D_s on reflection coefficients and gain variations in the horizontal plane (the *xy* plane). It can be seen that the antenna keeps a wide impedance bandwidth, and the bandwidth is not sensitive to the distance D_s. When D_s increases from 8 to 12 mm, the gain variation in the horizontal plane at 2.6 GHz is changed between 0.14 and 0.31 dB. Therefore, the distance D_s is chosen as 10 mm for the optimally designed back-to-back PFDAs. Also, the radiation characteristics, such as radiation patterns and peak gains, were measured within the operating band for the antenna, as shown in Figs. 22 and 23. Thanks to the quasi-omnidirectional radiation of the single PFDA, the back-to-back PFDAs achieve a desirable omnidirectional radiation performance in the horizontal plane with a flat gain variation of less than 1.27 dB. Moreover, a reasonably stable gain of around 2.2 dBi within the whole operating band is also obtained.

Table II compares the performances of the wideband back-to-back PFDAs with the recently published omnidirectional antennas. Designs in [14] and [17] are in the form of printed folded dipoles, and they have the moderate bandwidths of 20% and 55%. By employing planar coaxial collinear radiator [24] and multi-mode dielectric resonator [25], the flattest gain variations of 0.7 dB in the horizontal plane are achieved for these antennas. However, the series structure in [24] leads to a narrow bandwidth and a large size. In [25], a hybrid feed is used, which increases the complexity in the antenna design. By using modified monopole and dipole structures, antennas in [26] and [27] achieve very wide bandwidths in omnidirectional antenna designs. However, they suffer large gain variations in the horizontal plane. Through the above comparison, our proposed back-to-back PFDAs achieve a desirable flat gain variation (<1.27 dB) in the horizontal plane over a broad bandwidth (82%) with a compact size.

IV. CONCLUSION

A new approach to design wideband and compact multi-mode FDA is presented in this paper. By introducing shorting pins, CFSs, and parasitic patches on the planar folded dipole, three different resonant modes of the antenna can be excited and manipulated. By properly shifting these three

modes, the proposed antenna obtains a broad bandwidth of 80% and achieves a compact size of $0.3\lambda_0 \times 0.15\lambda_0 \times 0.05\lambda_0$. To validate the design concept, the antenna prototype is fabricated and measured. The experimental results are in good agreement with simulated results. Furthermore, a simple and effective design to realize omnidirectional radiation performance is presented by arranging two back-to-back PFDAs. The antenna exhibits a flat gain variation of less than 1.27 dB over a broad bandwidth (82%) in the horizontal plane. Such a compact, wideband, planar antenna is a promising candidate for many wireless applications, including indoor signal coverage, wireless access points, and micro base stations in 2G/3G/4G/5G and WLAN/WiMAX wireless communication systems.

REFERENCES

[1] A. R. Behera and A. R. Harish, "A novel printed wideband dipole antenna," *IEEE Trans. Antennas Propag.*, vol. 60, no. 9, pp. 4418–4422, Sep. 2012.

[2] L. Zhang, S. Gao, Q. Luo, P. R. Young, W. Li, and Q. Li, "Inverted-S antenna with wideband circular polarization and wide axial ratio beamwidth," *IEEE Trans. Antennas Propag.*, vol. 65, no. 4, pp. 1740–1748, Apr. 2017.

[3] L. Sun, Y. Li, Z. Zhang, and M. F. Iskander, "A compact planar omnidirectional MIMO array antenna with pattern phase diversity using folded dipole element," *IEEE Trans. Antennas Propag.*, vol. 67, no. 3, pp. 1688–1696, Mar. 2019.

[4] C. Ding, B. Jones, Y. J. Guo, and P.-Y. Qin, "Wideband matching of full-wavelength dipole with reflector for base station," *IEEE Trans. Antennas Propag.*, vol. 65, no. 10, pp. 5571–5576, Oct. 2017.

[5] L.-H. Wen *et al.*, "Compact dual-polarized shared-dipole antennas for base station applications," *IEEE Trans. Antennas Propag.*, vol. 66, no. 12, pp. 6826–6834, Dec. 2018.

[6] K. Ding, C. Gao, B. Zhang, Y. Wu, and D. Qu, "A compact printed unidirectional broadband antenna with parasitic patch," *IEEE Antennas Wireless Propag. Lett.*, vol. 16, pp. 2341–2344, 2017.

[7] Y. Yu, J. Xiong, and R. Wang, "A wideband omnidirectional antenna array with low gain variation," *IEEE Antennas Wireless Propag. Lett.*, vol. 15, pp. 386–389, Dec. 2015.

[8] L. Chang, L. L. Chen, J. Q. Zhang, and D. Li, "A broadband dipole antenna with parasitic patch loading," *IEEE Antennas Wireless Propag. Lett.*, vol. 17, no. 9, pp. 1717–1721, Sep. 2018.

[9] S.-G. Zhou, Z.-H. Peng, G.-L. Huang, and C.-Y. Desmond, "Design of a novel wideband and dual-polarized magnetoelectric dipole antenna," *IEEE Trans. Antennas Propag.*, vol. 65, no. 5, pp. 2645–2649, May 2017.

[10] X. Cui, F. Yang, M. Gao, L. Zhou, Z. Liang, and F. Yan, "A wideband magnetoelectric dipole antenna with microstrip line aperture-coupled excitation," *IEEE Trans. Antennas Propag.*, vol. 65, no. 12, pp. 7350–7354, Dec. 2017.

[11] J.-S. Roh, Y.-S. Chi, J.-H. Lee, Y. Tak, S. Nam, and T. J. Kang, "Embroidered wearable multiresonant folded dipole antenna for FM reception," *IEEE Antennas Wireless Propag. Lett.*, vol. 9, pp. 803–806, 2010.

[12] E. S. Ramon, S. Bernal, M. M. H. Armanious, J. S. Tyo, M. C. Skipper, and M. D. Abdalla, "Tunable electrically small conical folded dipole antenna used as a mesoband high-power microwave source," *IEEE Antennas Wireless Propag. Lett.*, vol. 15, pp. 1614–1617, 2016.

[13] I. J. Hwang, B. K. Ahn, S. H. Chae, J. W. Chae, and W. W. Lee, "Quasi-Yagi antenna array with modified folded dipole driver for mm wave 5G cellular devices," *IEEE Antennas Wireless Propag. Lett.*, vol. 18, no. 5, pp. 971–975, May 2019.

[14] F.-R. Hsiao and K.-L. Wong, "Omnidirectional planar folded dipole antenna," *IEEE Trans. Antennas Propag.*, vol. 52, no. 7, pp. 1898–1902, Jul. 2004.

[15] X. Cai and K. Sarabandi, "A compact broadband horizontally polarized omnidirectional antenna using planar folded dipole elements," *IEEE Trans. Antennas Propag.*, vol. 64, no. 2, pp. 414–422, Feb. 2016.

[16] R. Lampe, "Design formulas for an asymmetric coplanar strip folded dipole," *IEEE Trans. Antennas Propag.*, vol. AP-33, no. 9, pp. 1028–1031, Sep. 1985.

[17] S. Tanaka, Y. Kim, H. Morishita, S. Horiuchi, Y. Atsumi, and Y. Ido, "Wideband planar folded dipole antenna with self-balanced impedance property," *IEEE Trans. Antennas Propag.*, vol. 56, no. 5, pp. 1223–1228, May 2008.

[18] A. T. Mobashsher and A. Abbosh, "Slot-loaded folded dipole antenna with wideband and unidirectional performance for L-band applications," *IEEE Antennas Wireless Propag. Lett.*, vol. 13, pp. 798–801, 2014.

[19] A. T. Mobashsher and A. M. Abbosh, "Compact 3-D slot-loaded folded dipole antenna with unidirectional radiation and low impulse distortion for head imaging applications," *IEEE Trans. Antennas Propag.*, vol. 64, no. 7, pp. 3245–3250, Jul. 2016.

[20] N.-W. Liu, L. Zhu, and W.-W. Choi, "A low-profile wide-bandwidth planar inverted-F antenna under dual resonances: Principle and design approach," *IEEE Trans. Antennas Propag.*, vol. 65, no. 10, pp. 5019–5024, Oct. 2017.

[21] N.-W. Liu, L. Zhu, and W.-W. Choi, "A differential-fed microstrip patch antenna with bandwidth enhancement under operation of TM_{10} and TM_{30} modes," *IEEE Trans. Antennas Propag.*, vol. 65, no. 4, pp. 1607–1614, Apr. 2017.

[22] G. Thiele, E. Ekelman, and L. Henderson, "On the accuracy of the transmission line model of the folded dipole," *IEEE Trans. Antennas Propag.*, vol. AP-28, no. 5, pp. 700–703, Sep. 1980.

[23] C. A. Balanis, *Antenna Theory Analysis and Design*, 3rd ed. New York, NY, USA: Willey, 2005.

[24] Y. Chen, W. Hong, Z. Kuai, and H. Wang, "Ku-band linearly polarized omnidirectional planar filtenna," *IEEE Antennas Wireless Propag. Lett.*, vol. 11, pp. 310–313, Mar. 2012.

[25] P. F. Hu, Y. M. Pan, K. W. Leung, and X. Y. Zhang, "Wide-/dual-band omnidirectional filtering dielectric resonator antennas," *IEEE Trans. Antennas Propag.*, vol. 66, no. 5, pp. 2622–2627, May 2018.

[26] H. Huang, Y. Liu, and S. X. Gong, "Broadband dual-polarized omnidirectional antenna for 2G/3G/LTE/WiFi applications," *IEEE Antennas Wireless Propag. Lett.*, vol. 15, pp. 576–579, 2015.

[27] Z. Yang, J. Qiu, G. Teni, and S. Lin, "Design of a novel ultrawideband wire antenna with enhanced bandwidth," *IEEE Antennas Wireless Propag. Lett.*, vol. 11, pp. 624–627, 2012.

Wei Hu (S'09–M'13) received the Ph.D. degree in electromagnetic fields and microwave technology from Xidian University, Xi'an, China, in 2013.

From 2013 to 2017, he was a Lecturer with the National Key Laboratory of Antennas and the Microwave Technology, Collaborative Innovation Center of Information Sensing and Understanding, Xidian University, where he is currently an Associate Professor. From 2018 to 2019, he was an Academic Visitor with the University of Kent, Canterbury, U.K. He has authored or coauthored over 40 internationally refereed journal papers. His current research interests include multi-band and wideband antennas, circularly polarized antennas, MIMO antenna arrays, and wideband wide-scanning phased arrays.

Xuekang Liu received the B.S. degree in electronic and information engineering from Xidian University, Xi'an, China, in 2016, where he is currently pursuing the M.S. degree in electromagnetic fields and microwave technology.

His current research interests include wideband antennas, multi-mode antennas, and omnidirectional antennas.

Steven Gao (M'01–SM'16–F'19) received the Ph.D. degree in microwave engineering from Shanghai University, Shanghai, China, in 1999.

He is currently a Full Professor and the Chair of RF and microwave engineering, and the Director of Graduate Studies with the School of Engineering and Digital Arts, University of Kent, Canterbury, U.K. He has coauthored or coedited three books, *Space Antenna Handbook* (Wiley, 2012), *Circularly Polarized Antennas* (IEEE-Wiley, 2014), and *Low-Cost Smart Antennas* (Wiley, 2019), and over 300 papers. He holds ten patents. His current research interests include smart antennas, phased arrays, MIMO, reconfigurable antennas, wideband/multi-band antennas, satellite antennas, RF/microwave/mm-wave/THz circuits, mobile communications, satellite communications, UWB radars, synthetic aperture radars, Internet of Things (IoT), and sensors for healthcare.

Dr. Gao is a fellow of the Royal Aeronautical Society, U.K., and IET, U.K. He was a Distinguished Lecturer of the IEEE AP Society and is currently an Associate Editor of the IEEE TRANSACTIONS ON ANTENNAS AND PROPAGATION and several other international journals (*Radio Science*, IEEE ACCESS, *Electronics Letters*, *IET Circuits*, *Devices and Systems*, etc.), and the Editor-in-Chief of John Wiley & Sons Book Series on *Microwave and Wireless Technologies*. He was the General Chair of LAPC 2013 and an Invited Speaker at many conferences.

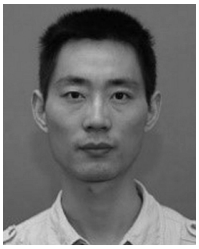

Lehu Wen received the M.S. degree from Xidian University, Xi'an, China, in 2011. He is currently pursuing the Ph.D. degree with the University of Kent, Canterbury, U.K.

His current research interests include multi-band base station antenna, mobile terminal antenna, and tightly coupled array.

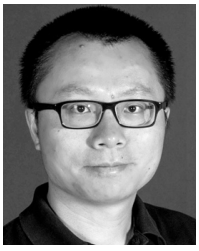

Qi Luo (S'08–M'12) received the Ph.D. degree (with distinction) from the University of Porto, Porto, Portugal, in 2012.

He is currently a Research Fellow with the School of Engineering and Digital Arts, University of Kent, Canterbury, U.K. His current research interests include smart antennas, circularly polarized antennas, reflectarray, transmitarray, multi-band microstrip antennas, and electrically small antennas. He has authored or coauthored two books, *Circularly Polarized Antennas* (Wiley-IEEE, 2014) and *Low-Cost Smart Antennas* (Wiley, 2019).

Dr. Luo was awarded as the Outstanding Reviewer for the IEEE TRANSACTIONS ON ANTENNAS AND PROPAGATION in 2015. He has been serving as a reviewer for a number of technical journals and international conferences.

Peng Fei (S'11–M'13) received the Ph.D. degree in electromagnetic wave and microwave technology from Xidian University, Xi'an, China, in 2013.

From 2013 to 2016, he was a Post-Doctoral Researcher with the Second Academy of China Aerospace Science and Industry Corporation, Beijing, China. In 2016, he joined the National Key Laboratory of Metrology and Calibration Technology, Beijing Institute of Radio Metrology and Measurement, Beijing, where he is currently a Senior Researcher. His current research interests include the design of antennas, feeding network and transceiver for wideband wireless systems, and millimeter-wave radar systems.

Yingzeng Yin (M'16) received the Ph.D. degree in electromagnetic wave and microwave technology from Xidian University, Xi'an, China, in 2002.

From 1990 to 1992, he was a Research Assistant and an Instructor with the Institute of Antennas and Electromagnetic Scattering, Xidian University, where he was an Associate Professor with the Department of Electromagnetic Engineering from 1992 to 1996, and has been a Professor since 2004. His current research interests include the design of microstrip antennas, feeds for parabolic reflectors, artificial magnetic conductors, phased array antennas, and computer-aided design for antennas.

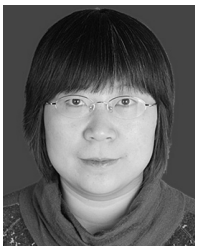

Ying Liu (M'09–SM'16) received the M.S. and Ph.D. degrees in electromagnetics from Xidian University, Xi'an, China, in 2001 and 2004, respectively.

From 2006 to 2007, she was a Post-Doctoral Researcher with Hanyang University, Seoul, South Korea. She is currently a Full Professor and the Director of the National Key Laboratory of Science and Technology on Antennas and Microwaves, Xidian University. She has authored or coauthored over 100 refereed journal papers and has authored *Prediction and Reduction of Antenna Radar Cross Section* (Xi'an: Xidian University Press, 2010) and *Antennas for Mobile Communication Systems* (Beijing: Electronics Industry Press, 2011). Her current research interests include antenna theory and technology, prediction, and control of antenna RCS.

Dr. Liu is a Senior Member of the Chinese Institute of Electronics. She was a recipient of the New Century Excellent Talents in the University of the Ministry of Education for China in 2011. She is a reviewer for several international journals and serves as a TPC member or the session chair for several IEEE flagship conferences.